Drug Design, Development and Therapy

Dovepress
open access to scientific and medical research

Open Access Full Text Article

ORIGINAL RESEARCH

Based on UPLC-Q-TOF/MS and Network Pharmacology to Explore the Mechanism of Qingre Lishi Decoction in the Treatment of Psoriasis

Jingjing Wei[1,*], Zhaoyang Liu[1,2,*], Mingming Li[1], Lingyun Du[1], Xia Zhu[1], Yi Leng[1], Changyu Han[1], Qingqing Xu[1], Chunhong Zhang[1]

[1]Department of Dermato-Venereology, the Second Hospital, Cheeloo College of Medicine, Shandong University, Jinan, People's Republic of China; [2]Department of Dermato-Venereology, Tianjin Medical University General Hospital, Tianjin, People's Republic of China

*These authors contributed equally to this work

Correspondence: Chunhong Zhang, Department of Dermato-Venereology, the Second Hospital, Cheeloo College of Medicine, Shandong University, 247 Beiyuan Dajie Street, Jinan, People's Republic of China, Tel +86-531-85875027, Fax +86-531-88962544, Email aliu133@163.com

Background: Psoriasis is an immune-mediated chronic inflammatory disease. Qingre Lishi Decoction (QRLSD) has achieved great clinical effect in the treatment of psoriasis. However, the potential bioactive components and the mechanisms are yet unclear.

Aim: To analyze the serum parameters of rats fed with QRLSD, screen out the active components of QRLSD, and explore the potential targets and pathway of QRLSD in the treatment of psoriasis.

Materials and Methods: The active components of serum containing QRLSD were analyzed using ultra-high performance liquid chromatography quadrupole-time-of-flight mass spectrometry (UPLC-Q-TOF/MS). The targets of QRLSD in the treatment of psoriasis were predicted by network pharmacology and molecular docking. In vitro experiments verified the underlying mechanism.

Results: By UPLC-Q-TOF/MS, 15 prototype components and 22 metabolites were identified in serum containing QRLSD. Subsequently, 260 chemical composition targets and 218 psoriasis targets were overlapped to obtain 23 intersection targets, including LGALS3, TNF, F10, DPP4, EGFR, MAPK14, STAT3 and others. TNF, IL-10, GAPDH, STAT3, EGFR, ITGB1, LGALS3 genes were identified as potential drug targets in the PPI network analyzed by CytoHubba. Gene Ontology (GO) and Kyoto Encyclopedia of Genes and Genomes (KEGG) analyses indicated that QRLSD may improve psoriasis by regulating immune and inflammatory pathways, the cytokine mediated signal transduction pathways and other signaling pathways. Molecular docking results showed that the main active components of the serum containing QRLSD had higher affinities for TNF and LGALS3. In vitro experiments confirmed that QRLSD may decrease levels of inflammatory cytokines by suppressing the NF-κB signaling pathway activated by TNF-α in human keratinocytes.

Conclusion: This study explores the potential compounds, targets and signaling pathways of QRLSD in the treatment of psoriasis, which will help clarify the efficacy and mechanism of QRLSD.

Keywords: qingre lishi decoction, psoriasis, UPLC-Q-TOF/MS, network pharmacology, molecular docking, NF-κB signaling pathway

Introduction

Psoriasis is a chronic skin disease characterized by erythema and desquamation. It is easy to relapse and significantly impacts patients' quality of life. The incidence rate in all ages ranged from 0.09% to 5.1%.[1] Although the environment, infection, neuropsychiatric, immune, and endocrine factors were considered to be related to pathogenesis of psoriasis, the precise cause remains elusive.[2] It can cause persistent inflammation, excess proliferation and dedifferentiation of keratinocytes, disordered autoimmunity, and increased angiogenesis through various immune mediations. At present, there are some optional treatments including topical corticosteroids, vitamin D analogues, calcineurin inhibitors,

Received: 16 May 2024
Accepted: 22 August 2024
Published: 28 August 2024

retinoids, phototherapy and biologics and so on. However, these treatments come with drawbacks, including recurrence, adverse reactions, high price, and limited applicability.[3,4]

Traditional Chinese Medicine (TCM) is widely utilized in the treatment of psoriasis. In TCM theory,[5] latent damp-heat syndrome permeates the development of psoriasis vulgaris. Damp-heat psoriasis is characterized by maculopapular eruption with obvious infiltration and more scales. According to the treatment of syndrome differentiation, TCM places emphasis on clearing heat and dampness, detoxifying and cooling blood in the treatment of damp-heat psoriasis. QRLSD is an efficacious TCM formula for treating psoriasis, composed of Flos Lonicerae (FL), Rhizoma Smilacis Glabrae (RSG), Radix Angelicae Sinensis, Radix Gentianae (RAS), and 16 additional herbal ingredients (as detailed in Table 1). Nevertheless, research on QRLSD is limited, and further investigation into its mechanism of action is warranted.

The efficacy of TCM is closely associated with serum pharmacokinetics, since only those compounds absorbed into the bloodstream can exhibit their pharmacological activities.[6,7] UPLC-Q-TOF/MS has proven to be a valuable tool for the identification of numerous components within complex matrices.[8] Hence, we used UPLC-Q-TOF/MS analysis to determine the absorbed phytochemical constituents and metabolites of QRLSD in the serum. Network pharmacology integrated drug targets and disease targets. Possible therapeutic targets or pathways are identified by KEGG and GO analysis.[9,10] Molecular docking may provide the interaction between a drug and its targets and predict its binding mode and affinity. However, due to the inherent limitations of virtual screening, these findings require validation through in vitro or in vivo studies. To investigate the potential key genes and pathways through which QRLSD acts on psoriasis, in vitro studies were conducted. The flowchart is illustrated in Figure 1.

Materials and Methods

Preparation of QRLSD

The 200 g QRLSD formulation was accurately weighed, the composition and proportion of medicinal herbs in the formula are shown in Table 1. The Affiliated Hospital of Shandong University of Traditional Chinese Medicine provided all these herbal materials. A volume of 2000 mL of water was added to the formula, which was then soaked for 30 minutes. This mixture was heated under reflux for another 30 minutes. The resulting liquid was filtered, and the residue was treated with 1600 mL of water. After a second round of heating and reflux for 25 minutes, the supernatants from both extractions were combined. Under reduced pressure, the combined extract was concentrated and subsequently freeze-dried to yield the freeze-dried powder of QRLSD. Accurately weighed 0.5g of freeze-dried powder and transferred into a stoppered conical flask. A solution

Table 1 Chinese Traditional Medical Herbs of QRLSD

Abbreviation	Medicinal Herbs	Original Plants	Proportion
FL	Flos Lonicerae	Lonicera japonica Thunb.	10
RSG	Rhizoma Smilacis Glabrae	Smilax glabra Roxb.	10
RAS	Radix Angelicae Sinensis	Angelica sinensis (Oliv.) Diels	3
RG	Radix Gentianae	Gentiana scabra Bunge	3
RS	Radix Scutellariae	Scutellaria baicalensis Georgi	3
RB	Radix Bupleuri	Bupleurum chinense DC.	3
RA	Rhizoma Alismatis	Alisma orientalis (Sam.) Juzep.	3
FG	Fructus Gardeniae	Gardenia jasminoides Ellis	3
PS	Plantain Seed	Plantago asiatica L. Plantago major L. Plantago depressa Willd.	5
DRR	Dried Rehmannia Root	Rehmannia glutinosa (Gaertn.) Libosch.ex Fisch. Et Mey.	5
CM	Cortex Moutan	Paeonia suffruticosa Andr.	5
RPR	Radix Paeoniae Rubra	Paeonia lactiflora Pall.	5
RL	Radix Lithospermi	Lithospermum erythrorhizon Sieb. et Zucc.	5
RI	Radix Isatidis	Isatis indigotica Fort.	10
FF	Fructus Forsythiae	Forsythia suspensa (Thunb.) Vahl	5
RGly	Radix Glycyrrhizae	Glycyrrhiza uralensis Fisch.	2

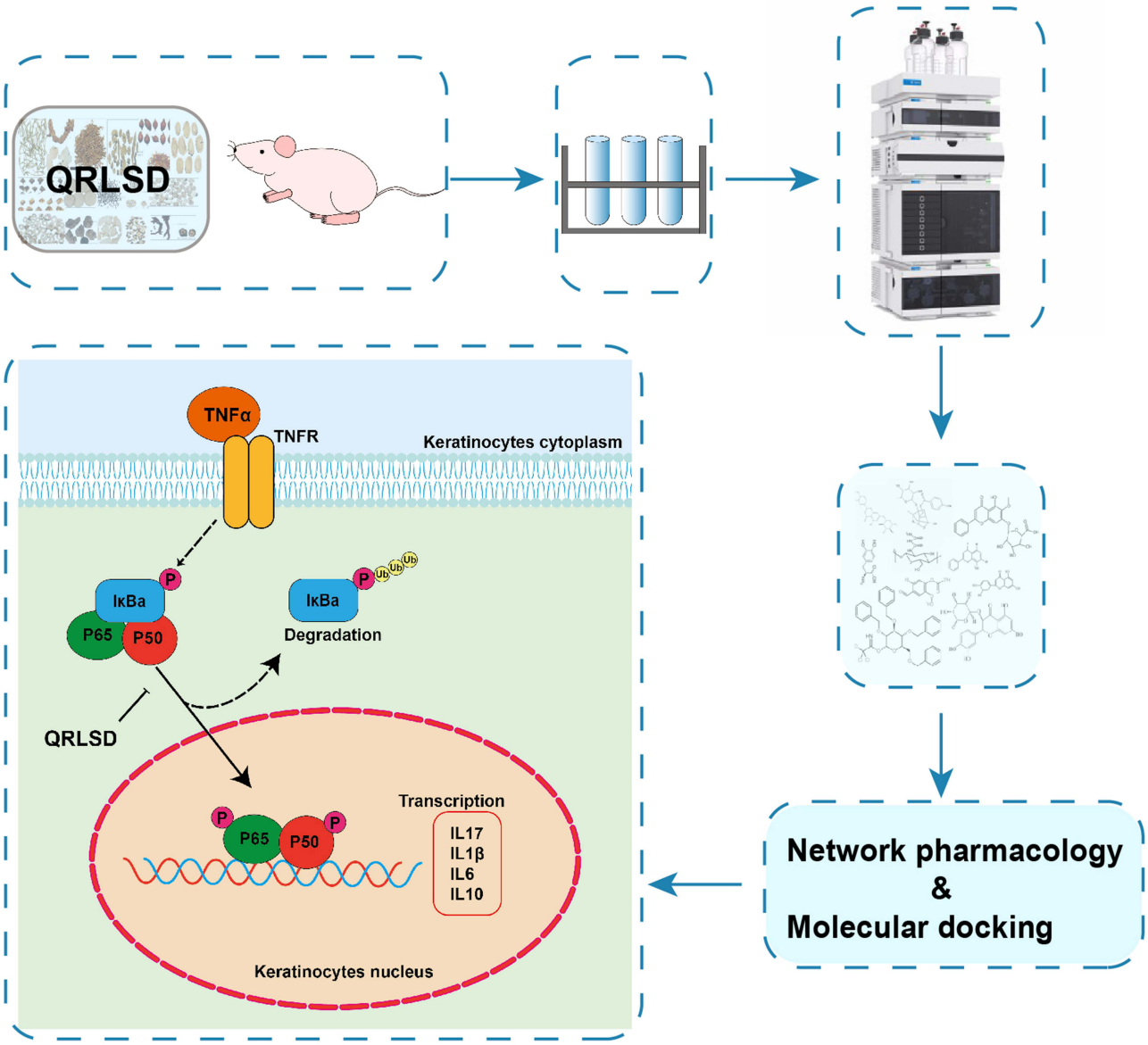

Figure 1 Flowchart of the study.

of 20 mL of 50% methanol was added to the flask. Following ultrasonic treatment at 300 W and 40 kHz for 30 minutes, the mixture was centrifuged at 12000 rpm for 5 minutes. The supernatant was collected to obtain the QRLSD extract.

Animals

Adult Sprague-Dawley (SD) rats, male, weighing between 170–190g, were purchased from Beijing Vital River Laboratory Animal Technology Co., Ltd. (Beijing, China) and housed in a pathogen-free facility at a temperature of 25 ± 5°C and 55 ± 5% humidity. Given these mice standard laboratory diet and water. All animal experiments followed the Guidelines for the Care and Use of Laboratory Animals. The Animal Care and Use Committee of the Second Hospital of Shandong University approved the animal experiment (KYLL2021(KJ)A-0424).

Preparation of Serum Samples for UPLC-Q-TOF-MS/MS

The healthy SD rats (170–190 g) were randomly divided into a blank group and a treatment group, with 3 rats in each group. Fasting for 12 h and drinking water freely before the experiment. The rats in the treatment group received an

intragastric administration of 10 g/kg body weight of QRLSD freeze-dried powder dissolved in 10 mL of solvent, while the blank control group was administered an equal volume of double-distilled water. The rats were anesthetized with ether, and 1 mL of blood was taken from the orbital venous plexus at 0 h, 0.5 h, 1 h and 2 h, respectively.[11] The serum was separated at 3000 rpm, and the serum samples at each time point were combined. Mixed serum samples with three times the volume of methanol (mass spectrometry grade) to precipitate proteins. After centrifugation (12,000 rpm, 4°C) for 5 minutes, the supernatant was transferred to new centrifuge tubes for subsequent concentration and drying. Added 80μL of 80% methanol to the residue for redissolving, mixed and centrifuged (12,000 rpm, 4°C) for 5 minutes, and took the supernatant for UPLC-Q-TOF-MS analysis. Upon completion of the experiment, the rats were humanely euthanized under deep anesthesia induced by an overdose of ether.

UPLC-Q-TOF-MS/MS Experimental Instruments and Reagents

Agilent 1290 UPLC ultra-high performance liquid chromatograph (Agilent Technologies Co., Ltd., USA); Agilent Q-TOF 6545 LC/MS high-resolution tandem mass spectrometry (Agilent Technologies Co., Ltd., USA); electronic analytical balance ME104 (Mettler-Toledo International Trading (Shanghai) Co., Ltd., China); high-speed centrifuge SIGMA3K15 (SIGMA, Germany); cleaning instrument KQ-300 BD (Kunshan Ultrasonic Instrument Co., Ltd., China); chromatographic column ACQUITY UPLC HSS T3 (Waters, USA); freeze-vacuum dryer (Boyikang Instrument Co., LTD., China), etc. QRLSD (Table 1) (batch number: NA, serial number: TS21C173-001, Shandong University of Traditional Chinese Medicine Hospital, China); Acetonitrile (I0928729804, Merck, USA); Methanol (I1139035113, Merck, USA); Formic acid (U9260048, CNW, Germany); Purified water (20210825C, Guangzhou Watsons Food & Beverage Co., Ltd., China).

Chromatographic and Mass Spectrometry Conditions

Chromatographic conditions: chromatographic column (No. SR011), Waters ACQUITY UPLC HSS T3 (1.8μm, 2.1mm×100mm); column temperature, 30 °C; Flow rate, 0.4 mL/min; injection volume, 2μL (serum sample); detection wavelength, 254 nm; mobile phase ratio: acetonitrile in phase A and 0.1% formic acid aqueous solution in phase B, gradient elution is presented in Supplementary Table S1. Electrospray Ionization Positive (ESI+) mode and Electrospray Ionization Negative (ESI-) mode were adopted for mass spectrometry, and the detailed mass spectrum parameters are shown in Table 2.[12,13]

Data Processing

During the identification process, mass spectrometry data was primarily matched with the PCDL database. Compounds were preliminarily screened according to the score information of each chromatographic peak, and further confirmed according to the primary and secondary information of each chromatographic peak. The compounds not included in the database were

Table 2 Mass Parameters of QRLSD by UPLC–Q-TOF/MS

MS	Parameter value	MS/MS	Parameter value
Mass Range	50~1700	MS/MS mass range	50~1700
Gas Temp (°C)	320	Collision Energy (eV)	20
Drying Gas (L/min)	8		
Nebulizer (psi)	35		
Sheath Gas Temp (°C)	350		
Sheath Gas Flow (L/min)	11		
Vcap (V)	4000		
Nozzle Voltage (V)	1000		
Fragmentor (V)	175		
Skimmer (V)	60		
Ref Mass	√pos 121.0508and922.0097 √neg 197.8073and1033.9881		

identified according to literature reports[14,15] and mass spectrum cracking rules. The data acquisition software is Agilent Q-TOF 6545 LC/MS, and the data processing software is Agilent Mass Hunter Qualitative Analysis B.07.00.

Network Pharmacology

Identification of Potential Targets of QRLSD Active Ingredients

The components present in both the control serum sample and the serum containing QRLSD were subtracted from the results of the UPLC-Q-TOF/MS analysis; the remaining components were considered to be the active constituents specific to the serum containing QRLSD. Molecular formulae and SMILES strings for these components were identified using PubChem (US National Institutes of Health, NIH. 2004. https://pubchem.ncbi.nlm.nih.gov/. Accessed Sept 2004). For the modified components without search results, we compared them with the analysis results of QRLSD liquid from our preliminary studies[12] and selected their corresponding prototype components. In total, 19 chemical ingredients were included in the analysis. The targets of ingredients were retrieved from the Traditional Chinese Medicine Systems Pharmacology Database and Analysis Platform (TCMSP. Lab of Systems Pharmacology. 2012. http://lsp.nwu.edu.cn/tcmsp.php. Accessed 2012). We used SwissTargetPrediction (Swiss Institute of Bioinformatics. http://swisstargetprediction.ch/) and Search Tool for Interacting Chemicals (STITCH. Max Planck Institute for Molecular Cell Biology and Genetics, Dresden. 2008. http://stitch.embl.de/. Accessed 2008). to predict the potential target genes for the compounds. For SwissTargetPrediction, the organism setting was specified as "Homo sapiens", and the threshold for 'gene probability' was set to greater than 0.6. In STITCH, the "minimum required interaction score" was adjusted to "high confidence (0.700)". Data meeting these criteria were aggregated for subsequent analysis.

Identification of Potential Psoriasis-Related Targets

The search term "psoriasis" was queried in the TCMSP, the Therapeutic Target Database (TTD. Bioinformatics and Drug Design group, Singapore. 2002. http://db.idrblab.net/ttd/. Accessed 2002). and Online Mendelian Inheritance in Man (OMIM. Johns Hopkins University, Baltimore. 1966. https://omim.org/. Accessed 1966). The results were synthesized and deduplicated to obtain potential targets associated with psoriasis. The targets of the ingredients of QRLSD drug-containing serum and psoriasis related targets were input into a Venn diagram generator (Venny, http://bioinformatics.psb.ugent.be/webtools/Venn/) to determine the overlapping targets between the two sets.

Construction of a Compounds-Genes Network for QRLSD

The overlapping targets were imported into Cytoscape version 3.9.0. In the generated network diagram, nodes represent both drug component compounds and disease-related genes, while edges denote the interactions between them. The thickness of the lines connecting the nodes could be used to represent the strength of the interactions. The size of a node indicates the number of lines connected to other nodes, so as to draw the "active ingredient-intersecting targets" network diagram.

Construction of Protein-Protein Interaction (PPI) Network

Many interactions between proteins are crucial to cellular processing and their systematic characterization can help elucidate the biology function.[16] To investigate these interactions, the selected overlapping target genes were uploaded to the "Multiple Proteins" section of the STRING v11.0 database (http://string-db.org). Here, the species was specified as "Homo sapiens". This allowed us to obtain the PPI network for the targets. Subsequently, this data was visualized using Cytoscape version 3.9.0. Each node's parameters were thoroughly assessed, and the connectivity was analyzed using the MCC algorithm within the cytoHubba plugin. From this analysis, the top 10 core overlapping target genes were identified and used to construct the interaction network.

Gene Ontology (GO) and Kyoto Encyclopedia of Genes and Genomes (KEGG) Pathway Enrichment

To gain deeper insights into the functions of the overlapping target genes, these genes were uploaded into the Database for Annotation, Visualization, and Integrated Discovery (DAVID) (https://david.ncifcrf.gov/), with the species was specified as "Homo Sapiens". The overlapping genes underwent functional enrichment analysis through GO and pathway enrichment analysis via the KEGG.

Molecular Docking

Molecular docking is a computational method that simulates the binding pattern of small molecules to biological macromolecules, enabling predictions of drug-target interactions at the molecular level. This technique is widely applied in the discovery of new drugs.[17] The key targets were selected based on the network diagram. The 2D structures of the requisite key components were retrieved from PubChem, while their 3D structures were obtained from Protein Data Bank (PDB, http://www.rcsb.org/pdb/home/home.do). These structures were preprocessed using the automated functions of MOE software, which involved removing water molecules, adding hydrogens, and modifying amino acids. Molecular docking was performed using AutodockVina v1.2.2 software. The docking results were visualized using PyMOL software to inspect the binding sites, identify the residues interacting with the ligand and display them in stick representation, adjust the color and angle of the protein, residues, and ligand, etc. It is commonly accepted that a binding energy less than zero signifies the spontaneous binding of a ligand molecule to a receptor protein. A binding energy lower than −5.0 kcal/mol suggests that the component exhibits favorable binding activity toward the target, while a binding energy below −7.0 kcal/mol indicates a strong binding affinity of the component for the target.

Preparation of QRLSD Drug-Containing Rat Sera

Healthy male SD rats were randomly assigned to either the control serum group (receiving the same volume of distilled water as the QRLSD dose) or the QRLSD serum group (administered 10 g of QRLSD freeze-dried powder dissolved in 10 mL of solution per kg body weight daily), with three rats per group. On the third day, one hour following the final administration, the rats were immobilized. Blood samples were collected from the retro-orbital venous plexus using sterile vacuum blood collection tubes. The samples were then centrifuged at 3000 rpm for 15 minutes. The resultant serum was heat-inactivated at 56°C for 30 minutes and subsequently filtered through a 0.22 μm sterile filter. The serum samples were stored at −80°C for future use.

Human Keratinocyte Culture and Treatment

Human immortalized keratinocytes (HaCaT cells) were acquired from Shanghai Fu Heng Biology (Shanghai, China) and cultured in modified Dulbecco's Modified Eagle Medium (DMEM) supplemented with 10% fetal bovine serum (FBS) and 1% penicillin-streptomycin solution. Cells were seeded in 12-well plates with medium containing either serum containing QRLSD or control serum and incubated at 37°C in a humidified atmosphere with 5% CO_2. The cells were respectively stimulated with tumor necrosis factor α (TNF-α) or interleukin-17A (IL-17A) at concentration of 10 ng/mL. Recombinant human TNF-α was purchased from PeproTech (Rocky Hill, NJ, USA). Following the treatment, both the cell supernatants and the cells themselves were collected for further analysis.

Real-Time Polymerase Chain Reaction

Total RNA was extracted using TRIzol Reagent (TaKaRa), and cDNA synthesis was carried out using the PrimeScript™ RT Reagent Kit (TaKaRa). Quantitative PCR (qPCR) analysis was performed on a real-time PCR system (Eppendorf) using the SYBR Green PCR Master Mix (TaKaRa). The expression levels of the target genes were normalized to β-actin levels, and the fold changes were calculated using the ΔΔCt method. The primer sequences utilized for qPCR are detailed in Table 3.

Table 3 qRT- PCR Primer

Gene	Forward	Reverse
IL-1β	ACTACAGCAAGGGCTTCAGG	GTGATCGTACAGGTGCATCG
IL-6	TCAATGAGGAGACTTGCCTGG	GGCTGGCATTTGTGGTTGG
IL-17A	GCCTTCAAGACTGAACACCG	TGACATGCCATTCCTCAGGG
IL-10	TCAAGGCGCATGTGAACTCC	GATGTCAAACTCACTCATGGCT
TNF-α	GGCCAAGCCCTGGTATGAG	GCTGAGTCGGTCACCCTTC

Immunofluorescence Staining

HaCaT keratinocytes were cultured on coverslips. The cells were then treated with medium containing either QRLSD serum or control serum and subsequently stimulated with TNF-α. Following the treatments, they were fixed with a mixture of ice-cold methanol and acetone (1:1 ratio) and incubated with 3% bovine serum albumin in PBS with 0.1% Triton X-100 for 20 minutes. After washing, immunofluorescence staining was performed using Nuclear factor-kappa B (NF-κB) phosphorylated p65 (p-p65, CST, 3033s) overnight at 4°C. The cells were then probed with secondary antibodies. Nuclei were stained with 4.6-diamidino-2-phenylindole (DAPI) (Beyotime, Shanghai, China) at a concentration of 2 μg/mL. Fluorescent images were captured using a laser scanning confocal microscope (LSM780, Zeiss, Oberkochen, Germany).

Elisa

Collect the supernatant from HaCaT cells stimulated with TNF-α or IL-17A for ELISA detection. Using ELISA kits from R&D Systems (Minneapolis, MN, USA), we measured the protein levels of interleukin-1β (IL-1β), interleukin-6 (IL-6), interleukin-10 (IL-10), IL-17A, and TNF-α in the culture samples according to the manufacturer's instructions.

Western Blot

Proteins were extracted from cells as described previously using an appropriate RIPA lysis buffer, and protein concentrations were measured using a BCA protein assay kit (Thermo Fisher Scientific, Waltham, USA). Proteins were then separated by 10% SDS-PAGE. The proteins were transferred from the gel to a PVDF membrane, which was subsequently blocked with 5% non-fat milk to prevent non-specific binding. The membranes were incubated overnight at 4°C with primary antibodies against NF-κB p65 (CST, #8242), phospho-NF-κB p65 (Ser536) (CST, #3033), and β-actin (Santa Cruz Biotechnology, sc-8432). Afterward, the membranes were incubated with peroxidase-conjugated secondary antibodies (1:5000 dilution). Finally, the blots were visualized using a chemiluminescence imaging analyzer (Tanon 5200, Shanghai, China) and analyzed with ImageJ software for quantification of protein bands. β-actin served as an internal reference.

Statistical Analysis

Except for the annotation analysis software, statistical analyses were conducted using unpaired *t*-tests with GraphPad Prism software (San Diego, CA, USA). Results are presented as the mean ± standard deviation (SD). To ensure reliability, each independent experiment was replicated a minimum of three times. When comparing significant differences among more than two groups, one-way ANOVA tests were employed. $P < 0.05$ was considered to be significant (*), and $P < 0.001$ was highly significant (***).

Results

Active Components of QRLSD Based on UPLC-Q-TOF-MS/MS

The test solution and reference solution were scanned under both ESI- and ESI+ modes by UPLC-Q-TOF/MS. Chromatographic information (chromatographic peak retention time, UV absorption characteristics, etc.) and mass spectrometry information (accurate relative molecular mass, fragmentation of secondary mass spectrometry, etc.) were compared against the control products. Possible molecular formulas were calculated, and structural formulas were deduced by integrating the natural product high-resolution mass spectrometry database and related literature.[14,15,18] The ESI- and ESI+ modes spectra for the blank group serum and the QRLSD-containing group serum are shown in Figure 2a–d, respectively. The differences between the two groups in the ESI- and ESI+ modes are shown in Figure 3a and b. As a result, compared with the prototype components of QRLSD obtained from previous studies,[12] 15 prototype components (Table 4) and 22 metabolites (Table 5) were identified from the QRLSD drug-containing serum samples.

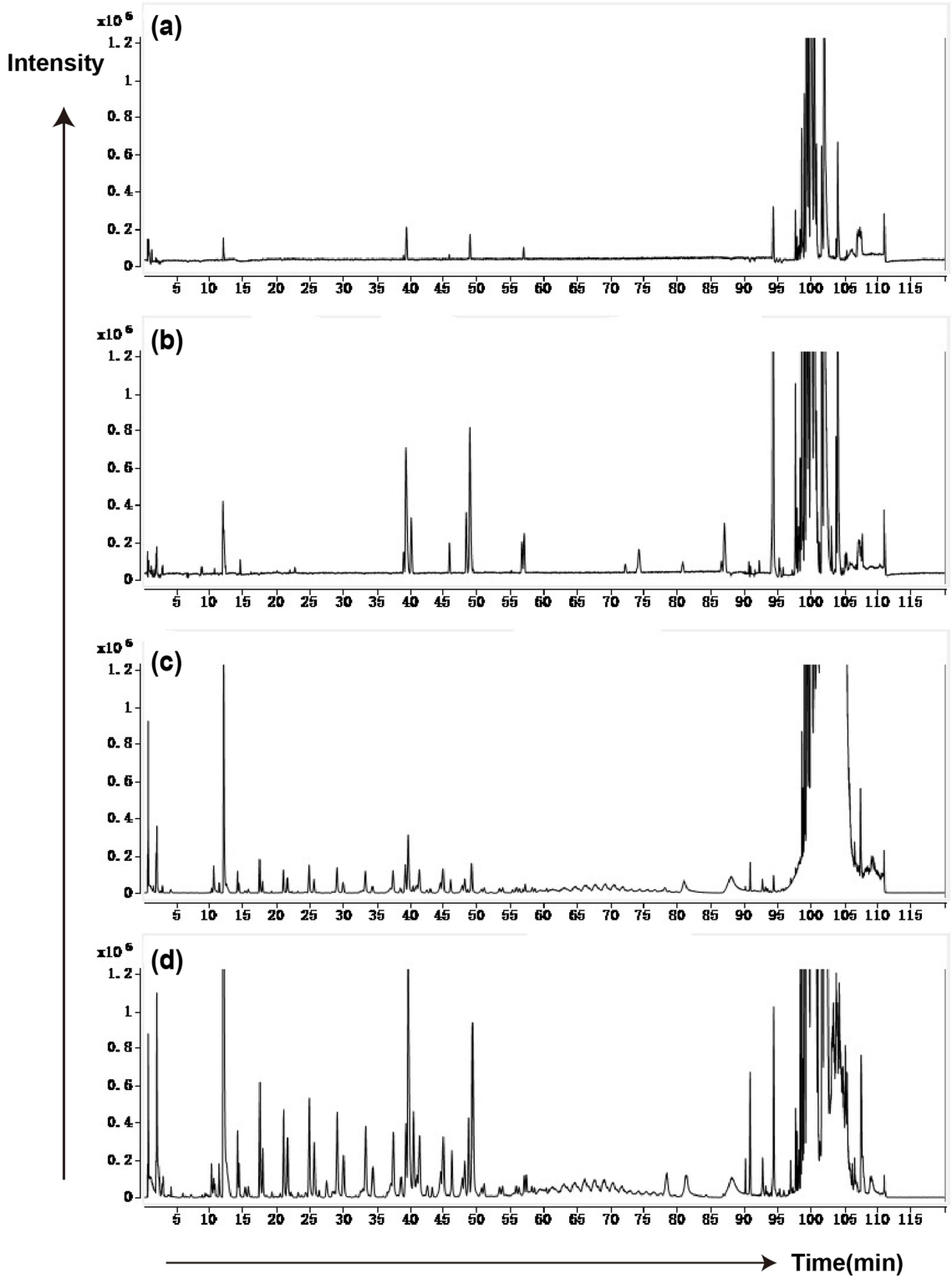

Figure 2 Extracted ion chromatograms (EIC) of serum samples based on UPLC-Q-TOF/MS. (**a**) Base peak chromatogram (BPC) of blank serum samples in ESI- mode, (**b**) BPC of QRLSD drug-containing serum samples in ESI- mode, (**c**) BPC of blank serum samples in ESI+ mode and (**d**) BPC of QRLSD drug-containing serum samples in ESI+ mode.

Network Pharmacology Analysis

Metabolites without conformation in PubChem were incorporated as their respective prototype components, and a total of 19 chemical components were included in this study. From the TCMSP, STITCH, and SwissTargetPrediction

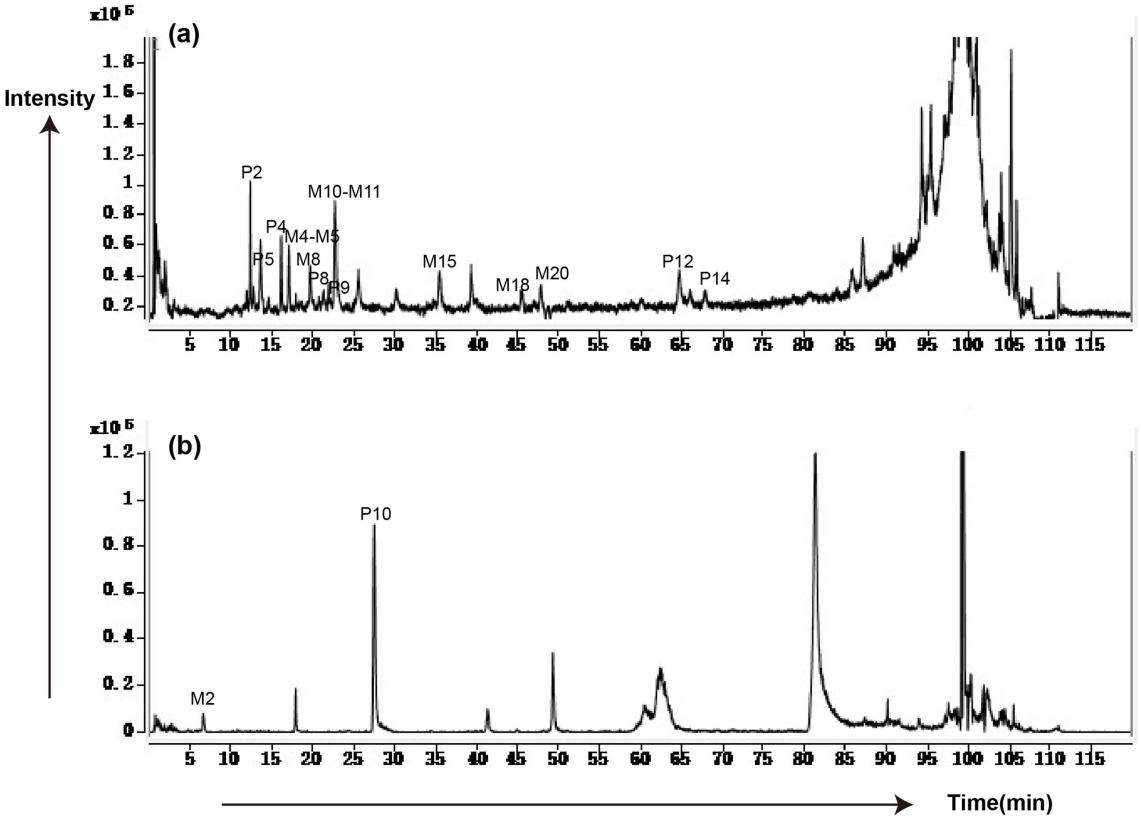

Figure 3 Extracted ion chromatograms (EIC) of active components of serum samples based on UPLC-Q-TOF/MS. (**a**) BPC in ESI- mode, (**b**) BPC in ESI+ mode.

databases, 260 targets of active ingredients of QRLSD were identified based on the predefined screening criteria. These targets were intersected with 218 "Psoriasis"-related targets obtained from TTD, OMIM, and TCMSP databases. 23 overlapping genes were identified as potential targets for QRLSD against psoriasis, as shown in the Venn diagram (Figure 4a), which includes genes such as mitogen activated protein kinase 14 (MAPK14), TNF, integrin beta-1 (ITGB1), dopamine receptor D2 (DRD2), arachidonate 5-lipoxygenase (ALOX5), protein tyrosine phosphatase non-receptor type 22 (PTPN22), IL10, signal transducer and activator of transcription 3 (STAT3) and others. (Supplementary Table S2).

To further explore the mechanism by which QRLSD may treat psoriasis, a network depicting "active components-disease targets" was constructed using Cytoscape version 3.9.0 software. This network consisted of 42 nodes and 59 edges (Figure 4b). Based on the degree centrality values, gentiopicroside, astilbin, debenzoylpaeoniflorin, caffeic acid, and wogonoside emerged as the principal bioactive components. Target proteins such as galectin-3 (LGALS3), TNF, coagulation factor X (F10), dipeptidyl peptidase-4 (DPP4), epidermal growth factor receptor (EGFR), and MAPK14 were found to be most intimately associated with the active substances present in the drug.

A PPI network, depicted in Figure 5a, was constructed to investigate the interaction landscape. The overlapping targets were then analyzed using the CytoHubba plugin within Cytoscape, screening for core gene hubs with the highest 10 scores, as illustrated in Figure 5b. The top five targets identified in this network were TNF, IL-10, glyceraldehyde-3-phosphate dehydrogenase (GAPDH), STAT3, and EGFR. These findings suggest that QRLSD may exert its therapeutic effects on psoriasis by modulating these critical targets.

The key overlapping targets were subjected to GO functional enrichment analysis by the DAVID database. This analysis resulted in the identification of 129 terms related to Biological Processes (BP), 20 terms related to Cellular Components (CC), and 18 terms related to Molecular Functions (MF). The top 10 enriched terms from each category were displayed in Figure 6a. QRLSD may affect cytokine mediated signaling pathways, signal transduction, positive regulation of gene expression, protein kinase B signaling, positive regulation of cell proliferation, and positive regulation of cell migration. KEGG pathway enrichment

Table 4 Identification Results of Prototype Components of Drug-Containing Plasma Samples

No	Time (min)	ESI	m/z actual value	*m/z* theoretical value	ppm	Formula	Molecular weight	Components	MS/MS
P1	8.47	$[M-H]^-$	315.1074	315.1085	−3.6	$C_{14}H_{20}O_8$	316.11	Vanilloloside	NA
P2	12.35	$[M-H]^-$	373.1136	373.1140	−1.2	$C_{16}H_{22}O_{10}$	374.12	Geniposidic acid	193.0493;167.0709;149.0604;123.0445
P3	13.43	$[M-H]^-$	375.1290	375.1297	−1.8	$C_{16}H_{24}O_{10}$	376.14	8-Epiloganic acid	375.1272;213.0755;169.0845;151.0761;125.0604 121.0646;59.0131
P4	13.58	$[M-H]^-$	165.0551	165.0557	−3.5	$C_9H_{10}O_3$	166.06	3-(4-Hydroxyphenyl) propionic acid	93.0334;59.0137
P5	16.83	$[M-H]^-$	375.1297	375.1297	−2.0	$C_{16}H_{24}O_{10}$	376.14	Loganic acid	375.1275;213.0745;89.0236;69.0331;59.0129
P6	18.69	$[M-H]^-$	495.1493	495.1508	−3.0	$C_{23}H_{28}O_{12}$	496.16	Oxypaeoniflorin	495.1487;137.0223
P7	19.40	$[M-H]^-$	373.1133	373.1140	−1.8	$C_{16}H_{22}O_{10}$	374.12	Secologanic acid	373.1471;193.0487;149.0602;97.0293;89.0233
P8	21.29	$[M+FA-H]^-$	401.1084	401.1089	−1.4	$C_{16}H_{20}O_9$	356.11	Gentiopicroside	401.1170;149.0587;89.0239;59.0132
P9	21.90	$[M+FA-H]^-$	433.1346	433.1351	−1.4	$C_{17}H_{24}O_{10}$	388.14	Geniposide	225.0753;207.0648;123.0443;101.0235
P10	27.49	$[M+H]^+$	226.1553	226.1550	1.2	$C_{11}H_{19}N_3O_2$	225.15	Plantagoguanidinic acid	226.1546;84.0558
P11	28.03	$[M-H]^-$	403.1238	403.1246	−1.9	$C_{17}H_{24}O_{11}$	404.13	Secoxyloganin	NA
P12	64.72	$[M-H]^-$	475.0877	475.0882	−1.1	$C_{22}H_{20}O_{12}$	476.10	Diosmetin 7-O-β-D-glucuronide	475.0875;299.0556;284.0321
P13	65.39	$[M-H]^-$	459.0922	459.0933	−2.4	$C_{22}H_{20}O_{11}$	460.10	Oroxylin A-7-O-glucuronide	NA
P14	67.85	$[M-H]^-$	459.0924	459.0933	−2.0	$C_{22}H_{20}O_{11}$	460.10	Wogonoside	283.0593;268.0362;113.0234
P15	92.69	$[M-H]^-$	821.3963	821.3965	−0.2	$C_{42}H_{62}O_{16}$	822.40	Glycyrrhizic acid	NA

Table 5 Identification Results of Metabolites of Drug-Containing Plasma Samples

No	Time (min)	ESI	m/z Actual value	*m/z* Theoretical value	ppm	Formula	Molecular weight	Components	MS/MS
M1	2.91	$[M+FA-H]^-$	421.1340	421.1351	−2.7	$C_{16}H_{24}O_{10}$	376.14	Debenzoylpaeoniflorin	421.0771;375.1261;345.1167;165.0546
M2	6.57	$[M+H]^+$	569.1689	569.1712	−4.0	$C_{22}H_{32}O_{17}$	568.16	Shanzhiside + glucuronidation	NA
M3	16.36	$[M-H]^-$	637.1985	637.1985	−0.1	$C_{26}H_{38}O_{18}$	638.21	Forsythoside E + glucuronidation	637.1944;461.1631
M4	17.01	$[M-H]^-$	258.9910	258.9918	−3.0	$C_9H_8O_7S$	260.00	Caffeic acid + sulfation	179.0343;135.0444
M5	17.10	$[M-H]^-$	355.0663	355.0671	−2.2	$C_{15}H_{16}O_{10}$	356.07	Caffeic acid + glucuronidation	NA
M6	18.42	$[M-H]^-$	625.1403	625.1410	−1.1	$C_{27}H_{30}O_{17}$	626.15	Astilbin + glucuronidation	625.1386;479.0834;449.1055;303.0498; 285.0377
M7	19.29	$[M-H]^-$	625.1403	625.1410	−1.2	$C_{27}H_{30}O_{17}$	626.15	Astilbin + glucuronidation	625.1379;479.0777;449.1052;303.0474; 285.0369
M8	19.65	$[M-H]^-$	273.0066	273.0074	−3.0	$C_{10}H_{10}O_7S$	274.01	Caffeic acid + methylation + sulfation	193.0498;178.0263;149.0601;134.0367
M9	22.13	$[M-H]^-$	609.1453	609.1461	−1.4	$C_{27}H_{30}O_{16}$	610.15	Engeletin + glucuronidation	433.1102;287.0551
M10	22.71	$[M-H]^-$	261.0069	261.0074	−1.9	$C_9H_{10}O_7S$	262.01	Caffeic acid + hydrogenation + sulfation	261.0059;181.0049;166.0267
M11	22.81	$[M-H]^-$	609.1449	609.1461	−2.1	$C_{27}H_{30}O_{16}$	610.15	Engeletin + glucuronidation	609.1462;433.1116;287.0548
M12	30.18	$[M-H]^-$	525.0340	525.0344	−0.8	$C_{21}H_{18}O_{14}S$	526.04	Baicalin + sulfation	525.0320;445.0734;349.0004;269.0444
M13	33.92	$[M-H]^-$	431.0978	431.0984	−1.2	$C_{21}H_{20}O_{10}$	432.11	Liquiritigenin + glucuronidation	NA
M14	34.74	$[M-H]^-$	497.0750	497.0759	−1.9	$C_{21}H_{22}O_{12}S$	498.08	Baicalein + hydrogenation + glucuronidation + sulfation	497.0715;417.1170;321.0423;241.0846?
M15	35.31	$[M-H]^-$	431.0977	431.0984	−1.6	$C_{21}H_{20}O_{10}$	432.11	Liquiritigenin + glucuronidation	NA
M16	38.91	$[M-H]^-$	445.0770	445.0776	−1.3	$C_{21}H_{18}O_{11}$	446.08	Baicalein + glucuronidation	269.0446;113.0239
M17	44.42	$[M-H]^-$	651.1198	651.1203	−0.7	$C_{28}H_{28}O_{18}$	652.13	Diosmetin + di-glucuronidation	651.1143;475.0852;299.0535
M18	45.46	$[M-H]^-$	621.1093	621.1097	−0.7	$C_{27}H_{26}O_{17}$	622.12	Baicalin + glucuronidation	621.0982;445.0760;269.0441
M19	47.01	$[M-H]^-$	621.1092	621.1097	−0.8	$C_{27}H_{26}O_{17}$	622.12	Baicalin + glucuronidation	445.0740;269.0442
M20	47.79	$[M-H]^-$	475.0875	475.0882	−1.4	$C_{22}H_{20}O_{12}$	476.10	Diosmetin + glucuronidation	NA
M21	51.16	$[M-H]^-$	651.1197	651.1203	−0.9	$C_{28}H_{28}O_{18}$	652.13	Diosmetin + di-glucuronidation	475.0857;299.0546
M22	66.06	$[M-H]^-$	445.0770	445.0776	−1.4	$C_{21}H_{18}O_{11}$	446.08	Baicalein + glucuronidation	445.0739;269.0444

https://doi.org/10.2147/DDDT.S467066 DovePress

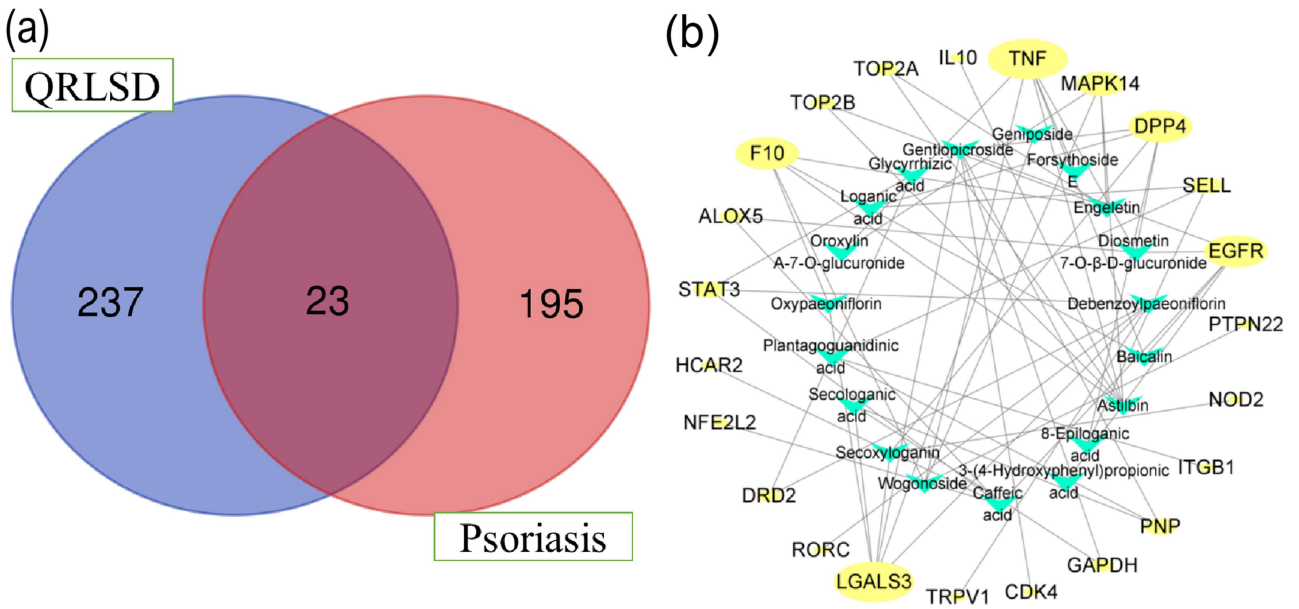

Figure 4 The first dimension-network pharmacology study of QRLSD in psoriasis. (**a**) Venn diagram of common targets in QRLSD and psoriasis. (**b**) The component-target network. The green arrows represent the compounds; the yellow round represent the genes; and edges represent the interactions. The line between two nodes represents the interaction, and the size of each node indicates the number of connections.

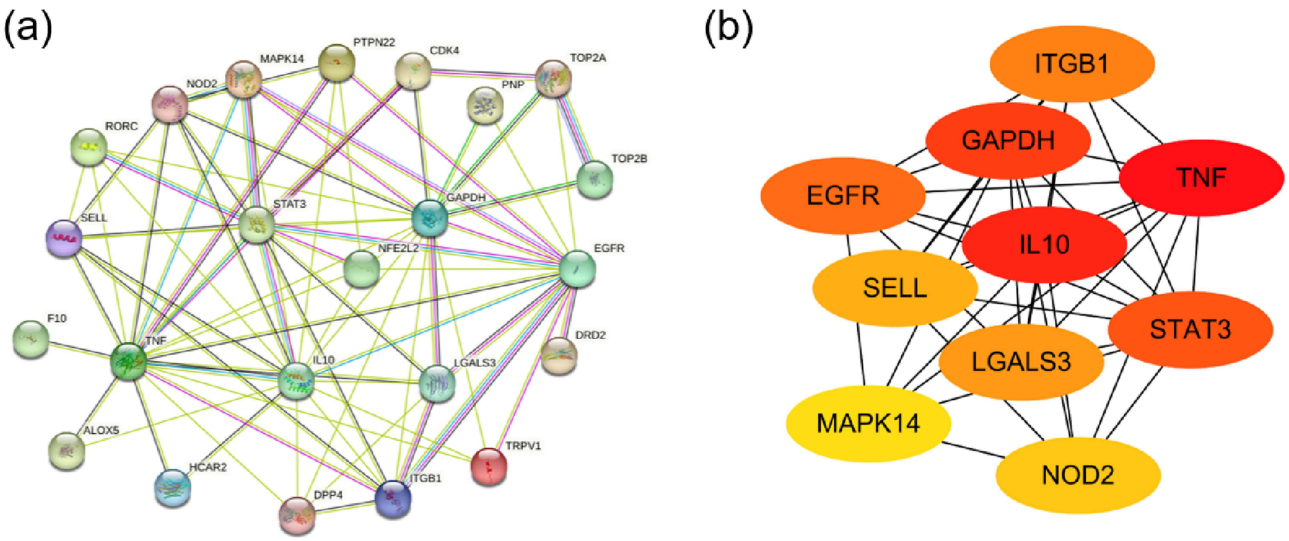

Figure 5 PPI network analysis. (**a**) PPI network of targets generated using STRING 11.0. Nodes represent proteins. Edges represent PPIs. (**b**) The 10 hub genes identified from the PPI network. The darker the color is, the more significant the gene.

analysis was also performed on overlapping targets using David database, yielding 40 significantly related pathways ($P < 0.05$), as shown in Figure 6b. QRLSD may regulate various immune-related diseases, inflammatory diseases and infectious diseases, such as cancer, inflammatory bowel disease, human cytomegalovirus infection, T cell receptor signaling pathway, TH17 differentiation pathway, etc.

Verification with Molecular Docking

Based on the drug-target correspondence, to further validate the primary active components of QRLSD, we conducted molecular docking studies involving TNF (Figure 7a–f) and LGALS3 (Figure 7g–l) with a variety of active ingredients, including astilbin, baicalin, diosmetin 7-O-β-D-glucopyranoside, forsythoside E, oroxylin A-7-O-glucuronide, wogonoside,

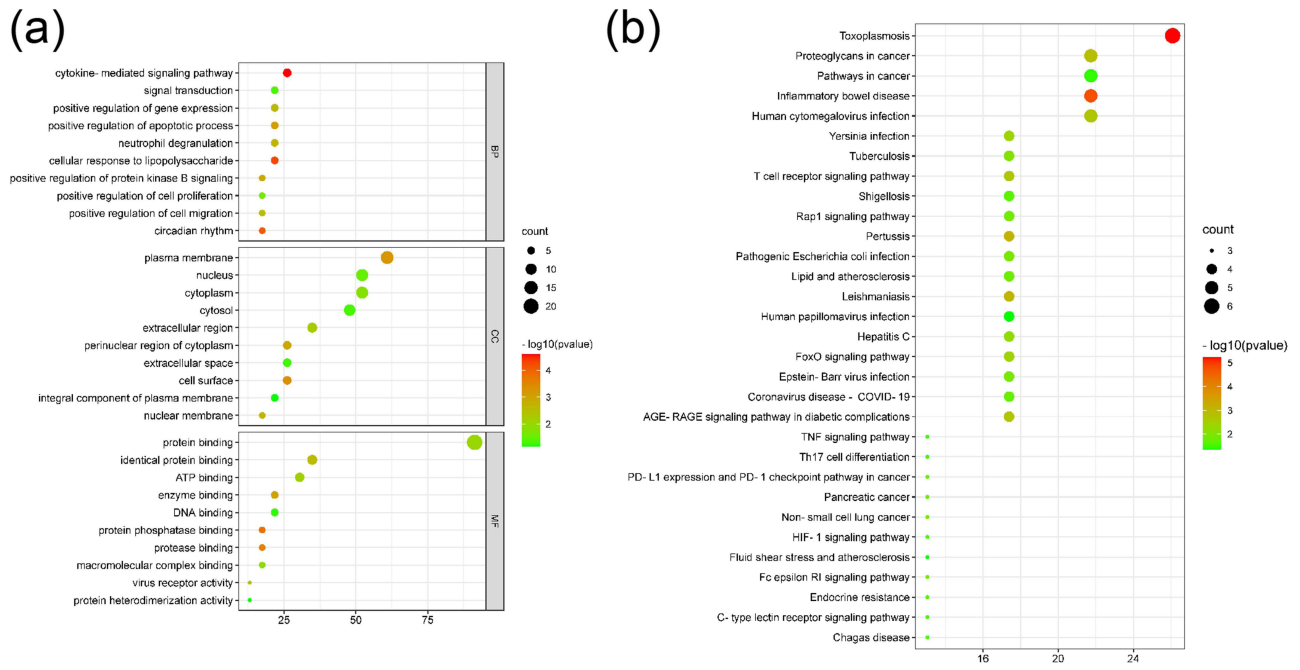

Figure 6 GO and KEGG pathway enrichment analysis results. (**a**) BP, CC and MF enrichment analysis; (**b**) KEGG enrichment analysis. X-axis represents the ratio of enriched target genes/background genes. Node color is displayed in a gradient from red to green in descending order of the P-value. The size of the nodes is arranged in ascending order of the number of genes.

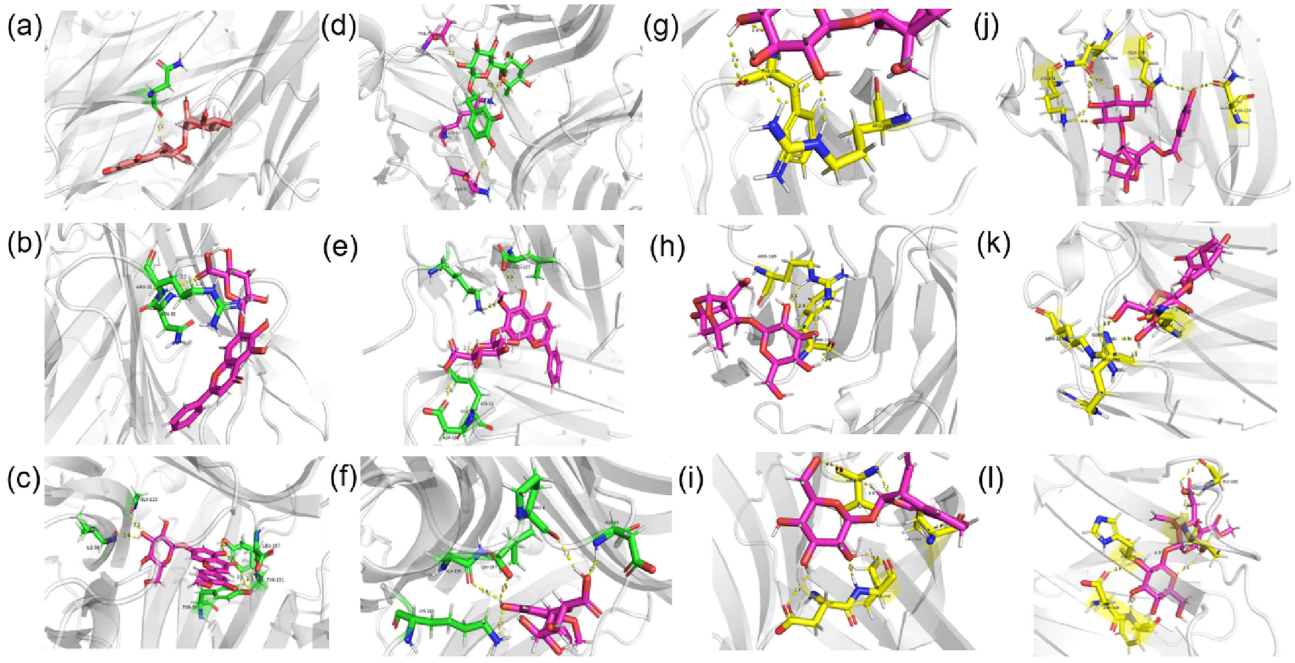

Figure 7 Molecular models of the binding of TNF with (**a**) Astilbin, (**b**) Baicalin, (**c**) Diosmetin 7-O-Beta-D-Glucopyranoside, (**d**) Forsythoside E, (**e**) Oroxylin A-7-O-glucuronide, (**f**) Wogonoside and LGALS3 with (**g**) Debenzoylpaeoniflorin, (**h**) Geniposide, (**i**) Gentiopicroside, (**j**) Oxypaeoniflorin, (**k**) Secologanic acid, (**l**) Secoxyloganin shown as 3D diagrams.

debenzoylpaeoniflorin, geniposide, gentiopicroside, oxypaeoniflorin, secologanic acid, and secoxyloganin. The results revealed that the binding energies were all less than −5 kcal/mol (Table 6), with the interaction between diosmetin 7-O-β-D-glucopyranoside and TNF exhibiting an especially low binding energy of −7.5439 kcal/mol.

Table 6 Docking Scores

Target Name	Bond Energy (Kcal/mol)	RMSD (Å)
Astilbin	−6.2698	1.5686
Baicalin	−6.034	0.7909
Diosmetin 7-O-β-D-Glucopyranoside	−7.5439	1.2331
Forsythoside E	−6.5510	1.5126
Oroxylin A-7-O-glucuronide	−6.5351	1.6897
Wogonoside	−6.3919	1.4714
Debenzoylpaeoniflorin	−5.1585	2.1123
Geniposide	−5.4579	1.7034
Gentiopicroside	−5.2779	1.9028
Oxypaeoniflorin	−6.2017	1.7162
Secologanic acid	−5.5425	1.5015
Secoxyloganin	−5.5512	2.1833

QRLSD Reduces the Expression of Proinflammatory Cytokines Through the TNF-α / NF-κB Signaling Pathway

With predictions from network pharmacology, we validated the most relevant genes and pathways. Network pharmacology suggested that TNF was essential target for QRLSD. As shown in Figure 8a–d, the expressions of IL-6, IL-1β and IL-17A

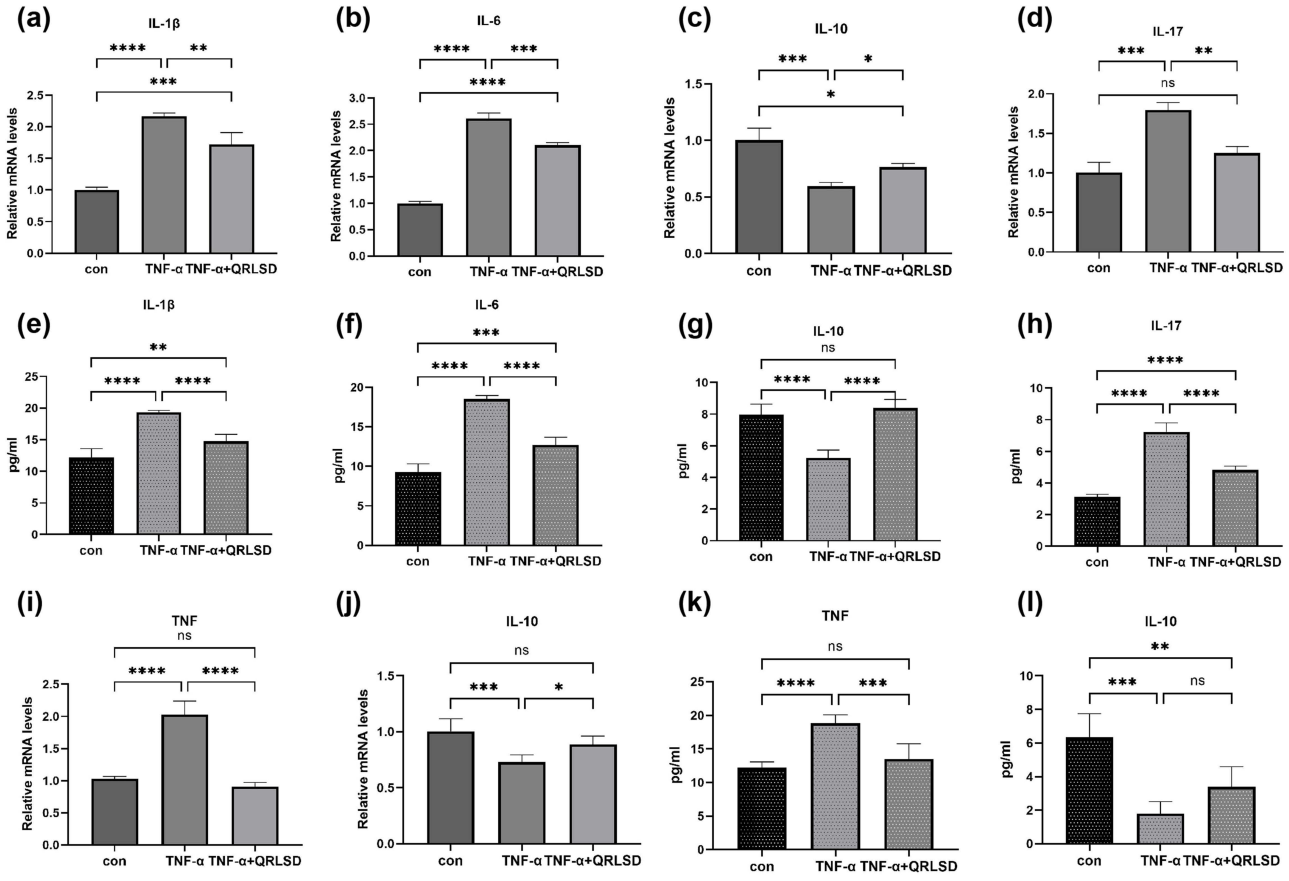

Figure 8 QRLSD inhibits inflammation by regulating the TNF/NF-κB signaling pathway in HaCaT keratinocytes. (**a–d**) IL-1β, IL-6, IL-10, IL-17A mRNAs Transcription Level in Keratinocytes Induced by TNF-α. β- actin served as a loading control. (**e–h**) ELISA was performed to assess the concentration of IL-1β, IL-6, IL-10, IL-17A in the supernatant of TNF-α-induced Keratinocytes pre-treated with or without QRLSD. (**i** and **j**) TNF-α, IL-10 mRNAs Transcription Level in Keratinocytes Induced by IL-17A. β-actin served as a loading control. (**k** and **l**) ELISA was performed to assess the concentration of TNF-α, IL-10 in the supernatant of IL-17A -induced Keratinocytes pre-treated with or without QRLSD. n=5 sample size. Data were expressed as mean ± SD. *P<0.05. **P<0.01. ***P<0.001. ****P<0.0001.

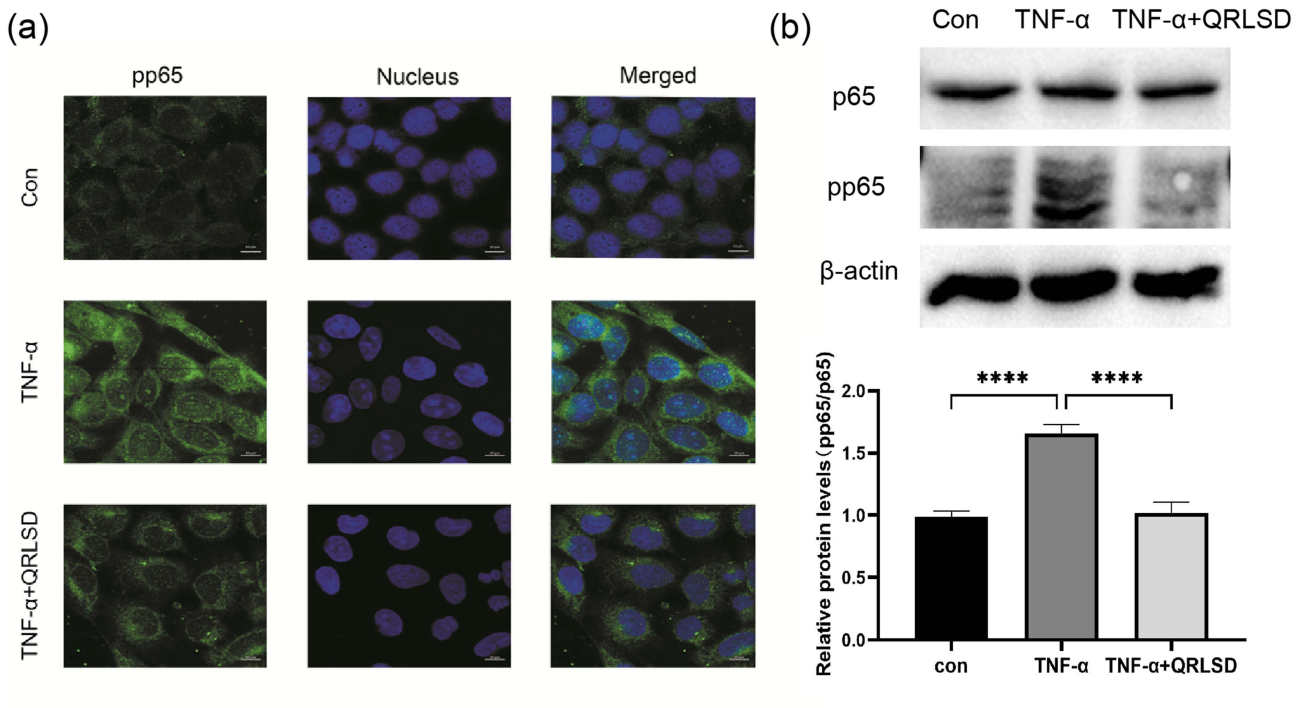

Figure 9 The Effect of QRLSD on p-p65 nuclear translocation in HaCaT keratinocytes stimulated by TNF-α. (**a**) Cells were fixed and IFA was carried out to detect p-p65 (green) distribution. Nuclei were stained with DAPI (blue). (**b**) Western blot analysis of p65 and p-p65 expression in TNF-α-induced Keratinocytes pre-treated or without QRLSD; β-actin served as a loading control. Data were expressed as mean ± SD. ****P<0.0001.

mRNA in HaCaT cells induced by TNF-α were significantly increased, and QRLSD treatment could significantly reduce the expression levels. Conversely, the expression of IL-10 mRNA exhibited an opposing trend. The content of inflammatory factors in the supernatant was detected (Figure 8e–h). The results were consistent with the mRNA changes. However, we stimulated HaCaT cells with IL-17A to mimic an inflammatory model, and the treatment with QRLSD was able to inhibit the secretion of TNF-α, as shown in Figure 8i–l. The NF-κB signaling pathway is known to play a critical role in the development of psoriasis.[19] In the control group, p-p65 was predominantly localized in the cytoplasm. Upon 2 hours of stimulation with TNF-α, there was a notable increase in the fluorescence intensity of p-p65 and a consequent translocation into the nucleus. However, QRLSD treatment sustained a reduced fluorescence intensity of p-p65 and inhibited its nuclear translocation, maintaining it in the cytoplasm, as depicted in Figure 9a. Western blotting (Figure 9b) further confirmed that QRLSD could significantly inhibit the increase of p-p65 expression in TNF-α-stimulated HaCaT cells.

Discussion

QRLSD is used in the treatment of moderate to severe plaque psoriasis. Through clinical observation, it has been found to achieve good clinical efficacy during all stages of the condition: the progressive phase, the stationary phase, and the regressive phase. Damp-heat latent syndrome runs through the development of plaque psoriasis, and QRLSD emphasizes clearing heat and dampness, purging fire and detoxifying, as well as cooling the blood and promoting its circulation. Typically, doctors prescribe the medication after performing a diagnosis through observation, auscultation and olfaction, inquiry, and palpation, taking into account individual patient differences. The patient then takes the prescription orally.

Our previous studies have shown that QRLSD can inhibit the proliferation of HaCaT cells and the development of imiquimod (IMQ)-induced psoriasis-like lesions in mice.[12] As a traditional Chinese medicine compound containing multiple components, QRLSD exerts its therapeutic effect on psoriasis through multiple targets, and this mechanism is complex to elucidate. In pharmacokinetics, compared with the study of drug components, studying blood-entry active components can provide more accurate analysis of specific drug component information than studying drug components alone, which helps to scientifically explain the biological effects of the drug. Therefore, we used UPLC-Q-TOF/MS to

separate, analyze, and identify the components of serum containing QRLSD, identifying 15 prototype components and 22 metabolites. Among these, 21 metabolites did not have conformations listed in PubChem, so their corresponding prototype components were selected. A total of 19 chemical components were included in this study, including astilbin, debenzoylpaeoniflorin, baicalin, gentiopicroside, caffeic acid, secologanic acid, and others (as shown in Figure 4b).

These active components have different biological characteristics. Some key active components can play various roles in the pathogenesis of psoriasis, such as the abnormal proliferation of HaCaT cells, inflammatory infiltration of immune cells, and immune regulation of T cells.[20–25] However, due to the complexity of TCM compounds and the limitations of component detection techniques in the past, the mechanisms by which many chemical components influence psoriasis have not been clear. Despite this, they have shown good biological efficacy in other immune-inflammatory-related diseases and common comorbidities of psoriasis,[23,26–30] which has become an important theoretical basis for reference.

As revealed in the core ingredients-core targets network and the visual analysis of PPI network, the following proteins may play notable roles: TNF, IL-10, GAPDH, STAT3, EGFR, LGALS3, etc. Among them, the important role of TNF in promoting inflammation has been confirmed.[31] In the early stage of psoriasis, innate immune cells are activated and secrete key cytokines such as TNF-α and INF-γ to activate myeloid dendritic cells.[32] Activated dendritic cells present antigens and secrete IL-12 and IL-23, resulting in Th1 and Th17 differentiation. Furthermore, the secretion of mediators such as TNF-α and IL-17A activates keratinocytes and promotes the secretion of inflammatory factors and chemokines, which further feedback to promote the cycle of inflammatory diseases and form an inflammatory cascade.[33–35] In addition, antagonizing TNF can also normalize the number of dendritic cells and reduce the expression of IL-17 and IL-23, and finally improve the histological manifestations.[36,37] In conclusion, TNF is a key cytokine in maintaining an inflammatory environment in psoriasis. Binding of TNF to its receptor TNFR1 activates TNF inflammatory signaling pathways, such as the classical NF-κB pathway.[38] Molecular docking results show that Astilbin, Baicalin, Diosmetin 7-O-beta-D-glucopyranoside, Forsythoside E, Oroxylin A glucuronide and Wogonoside has good docking activity with TNF. By binding to the core target, the active ingredient may affect the binding of TNF to its receptor, inhibit the TNF signal transduction pathway and downstream related inflammatory pathways, and ultimately lead to the reduction of the production of inflammatory factors.

The treatment of psoriasis by TCM compounds is holistic. Therefore, the related physiological processes of treating psoriasis with QRLSD may far exceed the predicted intersection targets and also involve other physiological processes related to the interactions of these targets. Through the enrichment analysis of GO biological functions, the most important biological processes include cytokine-mediated signaling pathways, neutrophil degranulation, and cell proliferation and apoptosis, which are consistent with the pathogenesis of psoriasis. KEGG enrichment analysis yielded 40 related pathways, many of which were involved in inflammation, immunity, and infection-related diseases. This may be related to the wide range of active ingredients in QRLSD and indicates that QRLSD has a strong effect on controlling inflammation.

The TNF signaling pathway obtained by enrichment analysis and the TNF targets with higher scores in the two network diagrams suggest that TNF is a relatively important target for the therapeutic effect of QRLSD. Inhibiting the signaling pathway mediated by this target may help regulate the homeostasis of the inflammatory environment. To investigate whether QRLSD influences the secretion of inflammatory cytokines through TNF-α, the expression levels and the content of the supernatant of inflammatory cytokines IL-6, IL-1β, IL-17A and IL-10 produced by TNF-α-induced HaCaT cells were examined. The results showed that IL-6, IL-1β and IL-17A produced by HaCaT cells induced by TNF-α was significantly down-regulated, while IL-10 was increased. After TNF-α stimulates keratinocytes, the phosphorylation of IκBkinases (IKKs) complex is activated, leading to the active expression of downstream NF-κB signaling pathway,[39] which then promotes the increased secretion of inflammatory factors. Through mouse models and genomic analysis of keratinocytes in vitro, it has been found that NF-κB is an essential nuclear transcription factor signal in the pathogenesis of psoriasis and is involved in the excessive proliferation of keratinocytes and inflammatory response.[19] p65 is a subunit of the NF-κB family, and its presence activates the NF-κB pathway, leading to increased transcriptional activity.[40] In the resting state, p65 binds to the pathway suppressor protein IκBα, located in the cytoplasmic. Upon stimulation, IκBα is phosphorylated and degraded, resulting in the release of p-p65 into the nucleus.[41] Therefore, by immunofluorescence and Western blotting analysis, it was observed that TNF-α stimulated p65 phosphorylation and its translocation into the nucleus. However, the p-p65 nuclear translocation was inhibited and its expression was reduced in

the group of serum containing QRLSD. After QRLSD acts on HaCaT cells pre-treated with IL-17A, the level of TNF-α in the supernatant decreases, while the level of IL-10 increases. This indicates that QRLSD may affects the positive feedback loop of inflammation, both inhibiting the production of TNF-α and the downstream NF-κB signaling pathway triggered by TNF.

Conclusions

This study, through UPLC-Q-TOF/MS, network pharmacology, and molecular docking analysis, identified potential targets for QRLSD in treating psoriasis: TNF, IL-10, GAPDH, STAT3, EGFR, LGALS3, and active components with possible anti-psoriatic effects: Astilbin, Baicalin, Debenzoylpaeoniflorin, Geniposide, among others. Our experimental validation suggests that QRLSD may exert an anti-inflammatory effect to treat psoriasis by inhibiting the TNF-α/NFκB pathway. However, the role of its active components in the pathogenesis of psoriasis remains unclear, which will be the focus of our future studies.

Abbreviations

QRLSD, Qingre Lishi Decoction; UPLC-Q-TOF/MS, ultra-high performance liquid chromatography quadrupole-time-of-flight mass spectrometry; SD, Sprague-Dawley; ESI+, Electrospray Ionization Positive; ESI-, Electrospray Ionization Negative; LGALS3, galectin-3; TNF-α, tumor necrosis factor α; F10, coagulation factor X; DPP4, dipeptidyl peptidase-4; EGFR, epidermal growth factor receptor; MAPK14, mitogen activated protein kinase 14; STAT3, signal transducer and activator of transcription 3; IL, interleukin; GAPDH, glyceraldehyde-3-phosphate dehydrogenase; ITGB1, integrin beta-1; DRD2, dopamine receptor D2; ALOX5, arachidonate 5-lipoxygenase; PTPN22, protein tyrosine phosphatase non-receptor type 22; PDB, Protein Data Bank; NF-κB, Nuclear factor-kappa B; p-p65, phosphorylated p65; TCM, Traditional Chinese Medicine; TCMSP, Traditional Chinese Medicine Systems Pharmacology Database and Analysis Platform; STITCH, Search Tool for Interacting Chemicals; TTD, Therapeutic Target Database; OMIM, Online Mendelian Inheritance in Man; PPI, protein-protein interaction; DAVID, Database for Annotation, Visualization and Integrated Discovery; GO, gene ontology; KEGG, Kyoto Encyclopedia of Genes and Genomes; CC, cell composition; MF, molecular function; BP, biological process; HaCaT, human immortalized keratinocytes; DMEM, Dulbecco's modified Eagle medium; FBS, fetal bovine serum; RT-PCR, Real-time polymerase chain reaction; DAPI, 4.6-diamidino-2-phenylindole; LSM, laser confocal microscopy; EIC, extracted ion chromatograms; BPC, base peak chromatogram.

Data Sharing Statement

Data will be made available on request from the corresponding author.

Ethics Approval and Consent to Participate

The animal study was reviewed and approved by The Second Hospital of Shandong University (KYLL2021(KJ)A-0424).

Acknowledgments

Part of this paper was uploaded to SSNR as a preprint: https://papers.ssrn.com/sol3/papers.cfm?abstract_id=4369310.

Funding

This work was supported by Shandong Natural Science Fund Joint Fund (ZR2021LZY005).

Disclosure

The authors report no conflicts of interest in this work.

References

1. Michalek IM, Loring B, John SM. A systematic review of worldwide epidemiology of psoriasis. *J Europ Acad Dermatol Venereol*. 2017;31(2):205–212. doi:10.1111/jdv.13854
2. Rendon A, Schäkel K. Psoriasis pathogenesis and treatment. *Int J Mol Sci*. 2019;20(6):1475. doi:10.3390/ijms20061475

3. Armstrong AW, Read C. Pathophysiology, clinical presentation, and treatment of psoriasis: a review. *JAMA*. 2020;323(19):1945–1960. doi:10.1001/jama.2020.4006
4. Bray JK, Cline A, Feldman SR. Assessing perceived adverse effects of biologic medications for patients with psoriasis. *J Am Acad Dermatol*. 2020;82(3):766–768. doi:10.1016/j.jaad.2019.11.002
5. Zhou N, Bai YP, Man XH, et al. Effect of new Pulian Ointment () in treating psoriasis of blood-heat syndrome: a randomized controlled trial. *Chin J Integr Med*. 2009;15(6):409–414. doi:10.1007/s11655-009-0409-0
6. Zhou TT, Zhu WJ, Feng H, et al. A network pharmacology integrated serum pharmacochemistry strategy for uncovering efficacy of YXC on hepatocellular carcinoma. *J Ethnopharmacol*. 2024;319(Pt 1):117125. doi:10.1016/j.jep.2023.117125
7. Du Y, Fan P, Zou L, et al. Serum metabolomics study of papillary thyroid carcinoma based on HPLC-Q-TOF-MS/MS. *Front Cell Develop Biol*. 2021;9:593510. doi:10.3389/fcell.2021.593510
8. Wong MY, So PK, Yao ZP. Direct analysis of traditional Chinese medicines by mass spectrometry. *J Chromatogr B Anal Technol Biomed Life Sci*. 2016;1026:2–14. doi:10.1016/j.jchromb.2015.11.032
9. Hao da C, Xiao PG. Network pharmacology: a Rosetta Stone for traditional Chinese medicine. *Drug Dev Res*. 2014;75(5):299–312. doi:10.1002/ddr.21214
10. Zhang R, Zhu X, Bai H, Ning K. Network pharmacology databases for traditional Chinese medicine. *Rev Assess Front Pharmacol*. 2019;10:123. doi:10.3389/fphar.2019.00123
11. Leblanc AF, Huang KM, Uddin ME, Anderson JT, Chen M, Hu S. Murine pharmacokinetic studies. *Bio-Protocol*. 2018;8(20):e3056. doi:10.21769/BioProtoc.3056
12. Zhu X, Xu Q, Liu Z, et al. Qingre Lishi Decoction ameliorates imiquimod-induced psoriasis-like skin lesions in SKH-1 mice by regulating the Treg-DC-Th17 axis and inhibiting MAPK-mediated DC maturation. *J Ethnopharmacol*. 2024;318(Pt A):116931. doi:10.1016/j.jep.2023.116931
13. Xu Q, Sheng L, Zhu X, et al. Jingfang granules exert anti-psoriasis effect by targeting MAPK-mediated dendritic cell maturation and PPARγ-mediated keratinocytes cell cycle progression in vitro and in vivo. *Phytomedicine*. 2023;117:154925. doi:10.1016/j.phymed.2023.154925
14. Yang R, Liu H, Bai C, et al. Chemical composition and pharmacological mechanism of qingfei paidu decoction and Ma Xing Shi Gan decoction against coronavirus disease 2019 (COVID-19): in silico and experimental study. *Pharmacol Res*. 2020;157:104820. doi:10.1016/j.phrs.2020.104820
15. Xue G, Zhu M, Meng N, et al. Integrating study on qualitative and quantitative characterization of the major constituents in shuanghuanglian injection with UHPLC/Q-Orbitrap-MS and UPLC-PDA. *J Analyt Meth Chem*. 2021;2021:9991363. doi:10.1155/2021/9991363
16. Scott DE, Bayly AR, Abell C, Skidmore J. Small molecules, big targets: drug discovery faces the protein-protein interaction challenge. *Nat Rev Drug Discov*. 2016;15(8):533–550. doi:10.1038/nrd.2016.29
17. Pinzi L, Rastelli G. Molecular docking: shifting paradigms in drug discovery. *Int J Mol Sci*. 2019;20(18):4331. doi:10.3390/ijms20184331
18. Xue Z, Yang B. Phenylethanoid glycosides: research advances in their phytochemistry, pharmacological activity and pharmacokinetics. *Molecules*. 2016;21(8):991. doi:10.3390/molecules21080991
19. Goldminz AM, Au SC, Kim N, Gottlieb AB, Lizzul PF. NF-κB: an essential transcription factor in psoriasis. *J Dermatological Sci*. 2013;69(2):89–94. doi:10.1016/j.jdermsci.2012.11.002
20. Di TT, Ruan ZT, Zhao JX, et al. Astilbin inhibits Th17 cell differentiation and ameliorates imiquimod-induced psoriasis-like skin lesions in BALB/c mice via Jak3/Stat3 signaling pathway. *Int Immunopharmacol*. 2016;32:32–38. doi:10.1016/j.intimp.2015.12.035
21. Xu Q, Liu Z, Cao Z, et al. Topical astilbin ameliorates imiquimod-induced psoriasis-like skin lesions in SKH-1 mice via suppression dendritic cell-Th17 inflammation axis. *J Cell & Mol Med*. 2022;26(4):1281–1292. doi:10.1111/jcmm.17184
22. Wang W, Yuhai, Wang H, Chasuna B. Astilbin reduces ROS accumulation and VEGF expression through Nrf2 in psoriasis-like skin disease. *Biol. Res.* 2019;52(1):49. doi:10.1186/s40659-019-0255-2
23. Sun Y, Zhang J, Huo R, et al. Paeoniflorin inhibits skin lesions in imiquimod-induced psoriasis-like mice by downregulating inflammation. *Int Immunopharmacol*. 2015;24(2):392–399. doi:10.1016/j.intimp.2014.12.032
24. Bai X, Yu C, Yang L, et al. Anti-psoriatic properties of paeoniflorin: suppression of the NF-kappaB pathway and Keratin 17. *Europ J Dermatol*. 2020;30(3):243–250. doi:10.1684/ejd.2020.3770
25. Hung CH, Wang CN, Cheng HH, et al. Baicalin ameliorates imiquimod-induced psoriasis-like inflammation in mice. *Planta med*. 2018;84(15):1110–1117. doi:10.1055/a-0622-8242
26. Yamada H, Kikuchi S, Inui T, Takahashi H, Kimura K. Gentiolactone, a secoiridoid dilactone from Gentiana triflora, inhibits TNF-α, iNOS and Cox-2 mRNA expression and blocks NF-κB promoter activity in murine macrophages. *PLoS One*. 2014;9(11):e113834. doi:10.1371/journal.pone.0113834
27. Czerwińska ME, Bobińska A, Cichocka K, Buchholz T, Woliński K, Melzig MF. *Cornus mas* and Cornus *officinalis*-a comparison of antioxidant and immunomodulatory activities of standardized fruit extracts in human neutrophils and caco-2 models. *Plants*. 2021;10(11):2347. doi:10.3390/plants10112347
28. Huang H, Cheng Z, Shi H, Xin W, Wang TT, Yu LL. Isolation and characterization of two flavonoids, engeletin and astilbin, from the leaves of Engelhardia roxburghiana and their potential anti-inflammatory properties. *J Agricult Food Chem*. 2011;59(9):4562–4569. doi:10.1021/jf2002969
29. Sun Y, Zhao Y, Yao J, et al. Wogonoside protects against dextran sulfate sodium-induced experimental colitis in mice by inhibiting NF-κB and NLRP3 inflammasome activation. *Biochem Pharmacol*. 2015;94(2):142–154. doi:10.1016/j.bcp.2015.02.002
30. Park SH, Jang S, Kim HK. Gardenia jasminoides extract ameliorates DfE-induced atopic dermatitis in mice through restoration of barrier function and T-helper 2-mediated immune response. *Biomed Pharmacothe*. 2022;145:112344. doi:10.1016/j.biopha.2021.112344
31. Lowes MA, Suárez-Fariñas M, Krueger JG. Immunology of psoriasis. *Ann Rev Immunol*. 2014;32:227–255. doi:10.1146/annurev-immunol-032713-120225
32. Ritter U, Meissner A, Ott J, Körner H. Analysis of the maturation process of dendritic cells deficient for TNF and lymphotoxin-alpha reveals an essential role for TNF. *J Leukoc Biol*. 2003;74(2):216–222. doi:10.1189/jlb.1202587
33. Chiricozzi A, Guttman-Yassky E, Suárez-Fariñas M, et al. Integrative responses to IL-17 and TNF-α in human keratinocytes account for key inflammatory pathogenic circuits in psoriasis. *J Investigat Dermatol*. 2011;131(3):677–687. doi:10.1038/jid.2010.340

34. Nadeem A, Ahmad SF, Al-Harbi NO, et al. Inhibition of interleukin-2-inducible T-cell kinase causes reduction in imiquimod-induced psoriasiform inflammation through reduction of Th17 cells and enhancement of Treg cells in mice. *Biochimie*. 2020;179:146–156. doi:10.1016/j.biochi.2020.09.023
35. Dominguez-Villar M, Hafler DA. Regulatory T cells in autoimmune disease. *Nat Immunol*. 2018;19(7):665–673. doi:10.1038/s41590-018-0120-4
36. Chen G, Goeddel DV. TNF-R1 signaling: a beautiful pathway. *Science*. 2002;296(5573):1634–1635. doi:10.1126/science.1071924
37. Mylonas A, Conrad C. Psoriasis: classical vs. paradoxical. the yin-yang of TNF and type i interferon. *Front Immunol*. 2018;9:2746. doi:10.3389/fimmu.2018.02746
38. Sethu S, Melendez AJ. New developments on the TNFα-mediated signalling pathways. *Biosci Rep*. 2011;31(1):63–76. doi:10.1042/BSR20100040
39. Yu H, Lin L, Zhang Z, Zhang H, Hu H. Targeting NF-κB pathway for the therapy of diseases: mechanism and clinical study. *Signal Transduc Target Therap*. 2020;5(1):209. doi:10.1038/s41392-020-00312-6
40. Hayden MS, Ghosh S. Regulation of NF-κB by TNF family cytokines. *Semin Immunopathol*. 2014;26(3):253–266. doi:10.1016/j.smim.2014.05.004
41. Hayden MS, Ghosh S. Shared principles in NF-kappaB signaling. *Cell*. 2008;132(3):344–362.